JPE 16-2-15

http://dx.doi.org/10.6113/JPE.2016.16.2.542
ISSN(Print): 1598-2092 / ISSN(Online): 2093-4718

An Improved Central 60° Synchronous Modulation for High Transient Performance with PMSM Stator Flux Control Used in Urban Rail Transit Systems

Xiaochun Fang†, Fei Lin*, and Zhongping Yang*

†,*School of Electrical Engineering, Beijing Jiaotong University, Beijing, China

Abstract

Central 60° synchronous modulation is an easy pulse-width modulation (PWM) method to implement for the traction inverters of urban rail trains at a very low switching frequency. Unfortunately, its switching patterns are determined by a Fourier analysis of assumed steady-state voltages. As a result, its transient responses are not very good with over-currents and high instantaneous torque pulses. In the proposed solution, the switching patterns of the conventional central 60° modulation are modified according to the dynamic error between the target and actual stator flux. Then, the specific trajectory of the stator flux and current vector can be guaranteed, which leads to better system transients. In addition, stator flux control is introduced to get smooth mode switching between the central 60° modulation and the other PWMs in this paper. A detailed flow chart of the control signal transmission is given. The target flux is obtained by an integral of the target voltage. The actual PMSM flux is estimated by a minimum order flux state observer based on the extended flux model. Based on a two-level inverter model, improved rules in the α-β stationary coordinate system and equations of the switching patterns amendment are proposed. The proposed method is verified by simulation and experimental results.

Key words: Central 60° synchronous modulation, Modulation modes switch, PMSM, Stator flux control, Transient response

I. INTRODUCTION

Medium-voltage high-power electric drive systems are used in the field of urban rail train drives. In order to keep the switching losses at a tolerable level, increase the output voltage and achieve a higher output power; the traction converter switching frequency is generally limited to a low range of several hundred Hz or less. As a result, multi-mode PWM (pulse-width modulation) is generally used [1], [2]. When the equivalent carrier ratio is low (10 or lower), special synchronous modulation is usually utilized. Unlike carrier-based PWM, special synchronous modulation generates a PWM wave by calculating the switching angles. The commonly used special synchronous modulation methods can be divided into two categories. The first class includes synchronous optimal modulation techniques, such as SHE-PWM (selective harmonic elimination-pulse width modulation) [3], [4]. The other class is made up of non-optimized special synchronous modulation techniques, such as central 60° synchronous modulation [5], [6].

The switching angle calculation of synchronous optimal modulation is complicated. The solution of transcendental equations is needed. For satisfying an objective function, a set of switching angles per fundamental period is determined for every steady-state operating point. When there are too many switching angles, the calculation becomes too complicated to be realized. Central 60° synchronous modulation generates switching angles without a current harmonic optimization objective function. There is only one switching angle that needs to be solved in central 60° synchronous modulation. Central 60° synchronous modulation is realized more easily than SHE-PWM. In addition, central 60° synchronous modulation has some outstanding merits such as quarter-wave symmetry and three-phase symmetry. Although it is not optimized precisely or strictly in terms of current harmonics; subharmonics, even harmonics and triplen harmonics are completely eliminated. It is able to output enough voltage

Manuscript received May 9, 2015; accepted Oct. 27, 2015
Recommended for publication by Associate Editor Bon-Gwan Gu.
†CorrespondingAuthor: me330221789@163.com
Tel: +86-10-51684864, Beijing Jiaotong University
*Dept. of Electrical Eng., Beijing Jiaotong University, China

© 2016 KIPE

fundamental amplitude and enters the square wave region smoothly. Central 60° synchronous modulation is an easily achieved method when the carrier ratio is relatively low in medium-voltage high-power electric drive systems.

The switching angles of the common central 60° synchronous modulation are a function of the fundamental voltage amplitude and the pulse number in each stator voltage fundamental period *N*. This function is deduced based on a steady-state voltage Fourier analysis for every steady-state operating point. Thus, the common central 60° synchronous modulation has poor transient response when the operating conditions change. Synchronous optimal modulation has analogously poor dynamic performance since the switching pattern calculation is also determined for every steady-state operating point. In an effort to promote the transient response of synchronous optimal modulation, the authors of [7], [8] proposed a stator current trajectory tracking approach. This strategy pursues the continuity of target and actual stator current harmonic vectors by fine-tuning to pre-calculated steady-state switching patterns in a dynamic process. Nevertheless, a fast identification of the motor inductance parameters is required to observe the harmonic currents. As a result, the stator current trajectory tracking approach is too difficult to be practical. A modified method, the stator flux trajectory control, which can avoid such complication, is then presented in [9], [10]. The stator flux is the control object in this modified strategy. The continuity of the target and actual stator flux is pursued by some modification in the steady-state switching patterns in a dynamic process. This modified method has a less sensitiveness to motor parameters, and the stator flux is easier to observe. Even more important is the fact that the continuity of the target and actual stator flux means the continuity of target and actual current vector in a dynamic process. Therefore, in this paper, the stator flux trajectory control is introduced to modify the switching angle calculation of the central 60° synchronous modulation for transient response improvement.

On the other hand, switching between different modulation modes is a key issue for achieving central 60° synchronous modulation. Little current impact should be ensured during a smooth mode switching. The commonly used solutions try to assure the continuity of the fundamental voltage phase and harmonic currents before and after mode switching [11], [12]. However, the way to keep fundamental voltage phase continuity is difficult to realize in low switching frequency digital control systems due to the time delay. Meanwhile, there are not many suitable ways to achieve harmonic current continuity in the commonly used solutions. The stator flux trajectory control is used to solve the modulation modes switch problem in this paper.

Among the various types of AC (alternating-current) motors, the PMSM (permanent magnet synchronous motor) has received widespread acceptance in industrial applications due to its high efficiency, high torque-to-current ratio, low noise, and robustness [13], [14]. This paper aims at PMSM control with multi-mode PWM in a wide fundamental frequency range with a low switching frequency. Central 60° synchronous modulation is used and modified by the stator flux trajectory control.

In Section 2, the principle of the common central 60° synchronous modulation is shown and the key question in terms of its transient response is pointed out. In Section 3, a detailed flow chart of the control signal transmission is given. Target flux calculation and actual PMSM flux observation methods are described in detail, unlike [9] and [10], where the model of the induction motor was the focus. More importantly, the basic rules of switching patterns modification to eliminate the flux error are proposed. In [9] and [10], dynamic flux error elimination is discussed in the three-phase stationary coordinate system. The three-phase flux error elimination is coupled. No specific solution is proposed for such a coupling relationship. Fast and accurate flux error elimination is difficult to achieve by this method. Some improvements are done in this paper, and dynamic flux error elimination will be discussed in the α-β stationary coordinate system. In addition, unlike the three-level inverter used in other approaches, a two-level inverter is employed in this paper, which results in a greater impact on the formulas. Simulation and the experimental verifications are presented in Section 4. Finally, come conclusions are drawn in Section 5.

II. Common Central 60° Modulation and Transient Response

A. Common Central 60° Synchronous Modulation

The generally used central 60° synchronous modulation contains situations where the pulse number *N* is 7, 5 or 3. For each phase voltage, the switching angles appear in π/3 to 2π/3 of a positive half-cycle and 4π/3 to 5π/3 of a negative half-cycle. The relationship between the pulsed voltage, modulation wave and equivalent carrier wave of central 60° synchronous modulation is shown in Fig. 1. Where, β_7, β_5 and β_3 are the switching angles when the pulse number *N* is 7, 5 and 3, respectively; T_s is the period of the modulation wave; T_c is the period of the equivalent carrier wave; U_{dc} is the voltage of the converter DC side; u_{Ao} is the A-phase voltage of a three-phase two-level inverter as an example; and ω_1 is the fundamental angular velocity. To simplify the switching angle calculation and digital control achievement, the switching angles in a steady-state cycle are assumed to be equal, no matter how many the pulse number *N* is. Every switching angle β is symmetrical about the central line of the corresponding equivalent carrier wave. When β_3 decreases to 0, the modulation mode enters square wave modulation naturally.

According to Fig. 1, the output pulsed voltage u_{Ao} of

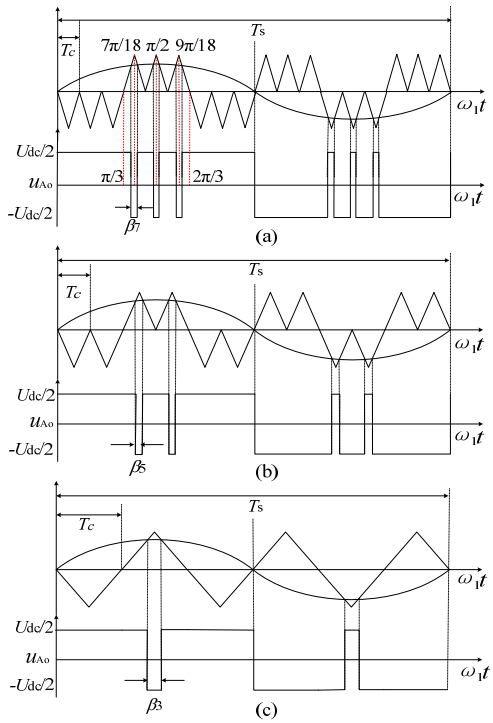

Fig. 1. Output voltage pulse of central 60° synchronous modulation. (a) N=7, (b) N=5, (c) N=3.

central 60° synchronous modulation has half-wave odd symmetry and quarter-wave symmetry. The functional relationship between the switching angle β and the fundamental voltage amplitude command U_1* is obtained from a Fourier analysis of pulsed voltage u_{Ao}. The Fourier analysis expression is:

$$u_{A0} = \sum_{n=1}^{\infty}\left[b_n \sin\left(n\omega_1 t\right)\right] \tag{1}$$

$$b_n = \frac{4}{\pi}\int_0^{\frac{\pi}{2}} u_{A0}(t)\sin\left(n\omega_1 t\right)d\left(\omega_1 t\right) \tag{2}$$

where, n is the harmonic order, and b_n is the harmonic amplitude. With the pulse number N=7 as an example, according to Equ. (2), the relationship between the fundamental amplitude b_1 and the switching angle β_7 is:

$$\begin{aligned} b_1 &= \frac{4}{\pi}\left[\begin{array}{l}\int_0^{\frac{7\pi}{18}-\frac{\beta_7}{2}}\frac{U_{dc}}{2}\sin\left(\omega_1 t\right)d\left(\omega_1 t\right)-\int_{\frac{7\pi}{18}-\frac{\beta_7}{2}}^{\frac{7\pi}{18}+\frac{\beta_7}{2}}\frac{U_{dc}}{2}\sin\left(\omega_1 t\right)d\left(\omega_1 t\right)\\ +\int_{\frac{7\pi}{18}+\frac{\beta_7}{2}}^{\frac{\pi}{2}-\frac{\beta_7}{2}}\frac{U_{dc}}{2}\sin\left(\omega_1 t\right)d\left(\omega_1 t\right)-\int_{\frac{\pi}{2}-\frac{\beta_7}{2}}^{\frac{\pi}{2}}\frac{U_{dc}}{2}\sin\left(\omega_1 t\right)d\left(\omega_1 t\right)\end{array}\right] \\ &= \frac{2U_{dc}}{\pi}\left[1-\left(4\sin\left(\frac{7\pi}{18}\right)+2\right)\sin\frac{\beta_7}{2}\right] \end{aligned} \tag{3}$$

In the motor control process, the reference fundamental voltage amplitude U_1* is given by the motor control. The switching angle β_7 can be calculated according to Equ. (3) with b_1= U_1*:

$$\beta_7 = 2\cdot\arcsin\left(\frac{1-\pi\cdot U_1^*/2U_{dc}}{4\sin\left(7\pi/18\right)+2}\right) \tag{4}$$

When N=5 and N=3, the switching angles β_5 and β_3 can be deduced in the same way.

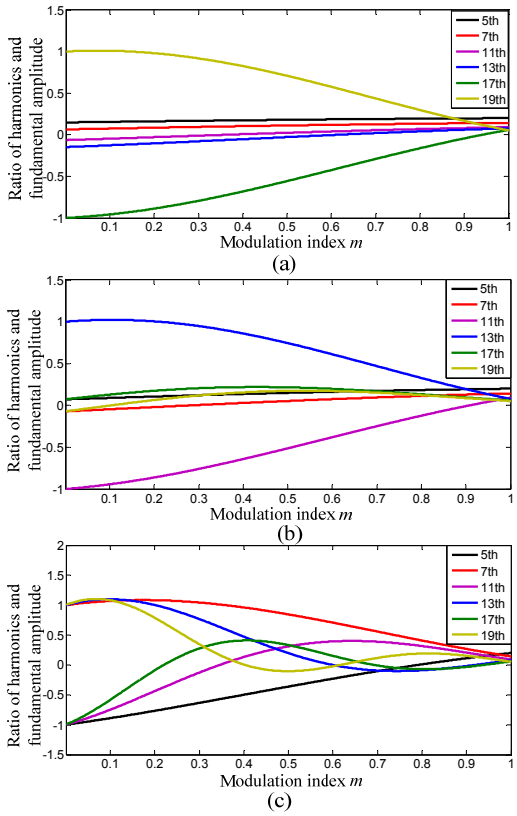

Fig. 2. Harmonic distribution of central 60° synchronous modulation output voltage. (a) N=7, (b) N=5, (c) N=3.

$$\beta_5 = 2\cdot\arcsin\left(\frac{1-\pi\cdot U_1^*/2U_{dc}}{\sqrt{2}+\sqrt{6}}\right) \tag{5}$$

$$\beta_3 = 2\cdot\arcsin\left(\frac{1-\pi\cdot U_1^*/2U_{dc}}{2}\right) \tag{6}$$

A specific switching pattern $P(\beta, N)$ is determined for each U_1* by Equs. (4)-(6), where the switch status changes with the fundamental phase angle.

The harmonic distribution of the central 60° synchronous modulation output voltage is shown in Fig. 2. In every subfigure, the abscissa is the modulation index m, and the ordinate is the ratio of the harmonics amplitude and the fundamental amplitude. The following conclusions can be obtained:

(1) There are no even harmonics or triplen harmonics.

(2) With different pulse number N, the main low order harmonics are different. Most crucially, their main harmonics content decreases when the modulation index m increases. Central 60° synchronous modulation is employed with a large m away from zero. The left half parts of the subfigures in Fig. 2 have no reference significance in practical applications.

Therefore, central 60° synchronous modulation can be used on occasions where the harmonic limit is not particularly strict. Its advantage is that it is easy to implement. However, the main focus of this paper is not there. Equations (4)-(6) are deduced based on a steady-state voltage Fourier analysis for

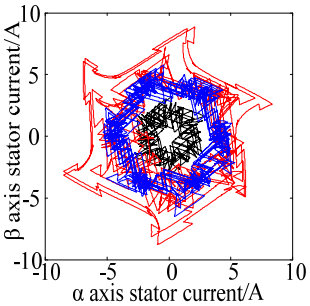

Fig. 3. Current trajectory in a dynamic adjustment process with load change.

every steady-state operating point. This means, each group U_1* and ω_1 of every sampling point is assumed to be constant in one cycle. However, this hypothesis is difficult to set up, especially under dynamic conditions. Therefore, when this method is used in a common digital control system, the motor performance will decline significantly.

B. Transient Response

The steady-state switching instants are well defined by the switching pattern $P(\beta, N)$ obtained from Equs. (4)-(6). In addition, the steady-state trajectory i_{hss} of the stator current harmonic vector is defined by the respective switching pattern. Therefore, this trajectory refers to steady-state operation. Any operation with a changing voltage reference is not steady state operation.

Assume the voltage reference changes at the time instant t_c. A different pulse pattern is then decided for inverter control. This also introduces a different current harmonic vector target trajectory. Immediately before the change, at $t=t_c^-$, the harmonic current is point $i_{hss}(t_c^-)$ on the old target trajectory. After the change, the harmonic current $i_{hss}(t_c^+)$ is defined by the new target trajectory. While the target point changes at t_c, the actual harmonic current maintains its value $i_h(t_c^-)$ at time instant t_c^+. The difference between the respective values before and after the change defines the dynamic error Δi_h of the stator current.

$$\Delta i_h = i_{hss}(t_c^+) - i_h(t_c^-) \tag{7}$$

The error is defined as a deviation of the harmonic current $i_h(t_c^-)$ at the instant of a commanded change from its target trajectory $i_{hss}(t_c^+)$, which is valid after the change under steady-state condition. The error vector appears instantaneously at t_c. It adds to the steady-state harmonic current of the new pulse sequences. Thus, it establishes a dc offset that decays in time. Subsequent errors may occur if the reference voltage continues changing. New error vectors are then added to the already existing errors from previous changes. The magnitude of the accumulated total error may eventually increase to values high enough to provoke an over-current trip. High instantaneous torque pulses are another consequence [9], [10]. As an example, the current trajectory in a dynamic adjustment process with a load change is shown in Fig. 3. The black, red, and blue parts correspond to the current trajectory before, during and after an adjustment, respectively. No special control, observable current ripple is existent in Fig. 3.

The stator current trajectory control, as a direct idea, aims at the essence of the transient problem. It is theoretically perfect to pursue the continuous harmonic current. A separation of the harmonic and fundamental currents is the key point of this method. Motor state equations are used repeatedly, and differential calculations are needed in the current observation. Therefore, the algorithm is complex and motor parameters sensitive.

Unlike the stator current trajectory control, the observation and control object of the stator flux trajectory control is the stator flux. The above vexing problem of the stator current trajectory control can be solved in the stator flux trajectory control. The relationship among the stator flux vector $\boldsymbol{\psi}_s$, the stator voltage vector $\boldsymbol{u}_s$ and the stator current vector $\boldsymbol{i}_s$ is:

$$\boldsymbol{u}_s = R_s \boldsymbol{i}_s + \frac{d\boldsymbol{\psi}_s}{dt} \tag{8}$$

where, R_s is the stator resistance. Therefore, not considering the minor influence of the stator resistance, the stator flux trajectory is parameter independent. In addition, there is a linear relationship between the stator flux and current, as shown in Equ. (9):

$$\boldsymbol{\psi}_s = L_s \boldsymbol{i}_s + \boldsymbol{\psi}_f \tag{9}$$

where, L_s is the stator inductance, and ψ_f is the rotor flux generated by the permanent magnet of a PMSM. Harmonic current continuity can be ensured with stator flux tracking. Therefore, the previously mentioned transient problem of central 60° synchronous modulation can be solved theoretically by the stator flux trajectory control.

III. Central 60° Synchronous Modulation Revised by the PMSM Stator Flux Trajectory Control

As previously mentioned, for each group U_1* and ω_1, a specific switching pattern $P(\beta, N)$ is determined in central 60° synchronous modulation. As a result, the stator flux vector follows a trajectory that can be considered a target. Similar to the stator current trajectory, the trajectory of the stator flux vector holds a short-time history of the operating conditions of the motor. Therefore, there is a stator flux vector error between the target and actual one when the reference fundamental voltage U_1* changes. A modification of the switching pattern $P(\beta, N)$ is proposed to eliminate the dynamic flux error in the transient state. A signal flow graph of stator flux trajectory control is shown in Fig. 4. It is built around the traditional PMSM control with central 60° synchronous PWM by adding a target stator flux calculation module, an estimator of the actual PMSM stator flux, and a switching pattern $P(\beta, N)$ modification module.

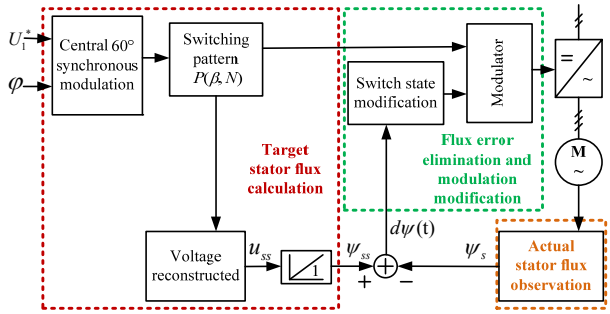

Fig. 4. Stator flux trajectory control signal flow graph.

A. Target Stator Flux Trajectory Calculation

The target stator flux ψ_{ss} is obtained from the actual pulse pattern [9], [10]. A stationary waveform of the stator voltage vector $u_{ss}(t)$ can be reconstructed from the specific switching pattern $P(\beta, N)$ and the stator frequency ω_1. Assuming that a transient is commanded at time instant t_c, the pulse pattern must change from $P_{past}(\beta, N)$ to $P_{new}(\beta, N)$. Therefore, $u_{ss}(t)$ changes from $u_{sspast}(t)$ to $u_{ssnew}(t)$ at t_c. The target steady-state stator flux trajectory $\psi_{ssnew}(t)$ after time t_c is:

$$\psi_{ssnew}(t) = \int_{t_c}^{t} u_{ssnew}(t)dt + \psi_{ssnew}(t_c) \tag{10}$$

where, $\psi_{ssnew}(t_c)$ is the initial value at the instant t_c of the pattern change. The initial value $\psi_{ssnew}(t_c)$ depends on the phase angle $\varphi(t_c)$ of the reference voltage vector at the time instant t_c. $\psi_{ssnew}(t_c)$ is determined as:

$$\psi_{ssnew}(t_c) = \int_{0}^{t_c} u_{ssnew}(t)dt - \psi_{ssnew}(\varphi = 0) \tag{11}$$

where, the integral start time 0 corresponds to the voltage phase 0, which is a virtual time look back from t_c with the phase angle changing of $u_{ssnew}(t)$. There is a dc bias of the integral part in Equ. (11). $\psi_{ssnew}(\varphi=0)$ in Equ. (11) is a correction of the integral part, which ensures that the average value of the steady-state flux in one cycle is zero. $\psi_{ssnew}(\varphi=0)$ is calculated by Equ. (12).

$$\psi_{ssnew}(\varphi = 0) = \int_{0}^{2\pi} \psi_{ssnew}(\varphi)d\varphi \Big/ 2\pi \tag{12}$$

B. Actual Stator Flux Trajectory Observation

The actual stator flux ψ_s is estimated by a minimum order flux state observer based on the extended flux model.

The voltage equation of an interior PMSM can be expressed as:

$$\begin{bmatrix} u_q \\ u_d \end{bmatrix} = \begin{bmatrix} R_s + DL_q & -\omega_r L_q \\ -\omega_r L_q & R_s + DL_q \end{bmatrix} \begin{bmatrix} i_q \\ i_d \end{bmatrix} + \begin{bmatrix} 0 \\ (L_d - L_q)DL_q \end{bmatrix} + \omega_r \begin{bmatrix} \psi_f + (L_d - L_q)i_d \\ 0 \end{bmatrix} \tag{13}$$

where, u_d and u_q are d- and q-axis components of the stator voltage; L_q and L_d are the d- and q-axis components of the inductance; i_d and i_q are the d- and q-axis components of the stator current; and ω_r is the electrical rotor angle velocity. The last matrix of Equ. (13) is the extended flux ψ_e. A minimum order rotor flux position state observer based on the extended flux model is proposed in [15]. By chaning the coordinate system of Equ. (13), a voltage equation in the α-β stationary coordinate system can be obtained.

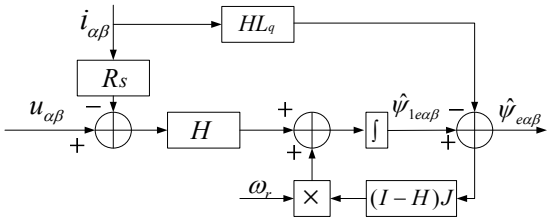

Fig. 5. State observer structure of extended flux.

$$\begin{cases} u_{\alpha\beta} = R_s i_{\alpha\beta} + L_q D i_{\alpha\beta} + D\psi_{e\alpha\beta} \\ u_{\alpha\beta} = \begin{bmatrix} u_\alpha & u_\beta \end{bmatrix}^T \\ i_{\alpha\beta} = \begin{bmatrix} i_\alpha & i_\beta \end{bmatrix}^T \\ \psi_{e\alpha\beta} = \begin{bmatrix} \psi_{e\alpha} \\ \psi_{e\beta} \end{bmatrix} = \begin{bmatrix} \psi_f + (L_d - L_q)i_d \end{bmatrix} \begin{bmatrix} \cos\theta \\ \sin\theta \end{bmatrix} \end{cases} \tag{14}$$

In Equ. (14), D is the differential operator. The first equation of Equ. (14) is the key to observe the extended flux. The main calculation process is expressed by Equ. (15). $-\rho$ is the pole of the observation error equation, and I is the unit matrix.

$$\begin{cases} \hat{\psi}_{e\alpha\beta} = \hat{\psi}_{1e\alpha\beta} - HL_q i_{\alpha\beta} \\ D\hat{\psi}_{1e\alpha\beta} = \omega_r (H - I)J\hat{\psi}_{e\alpha\beta} + H(u_{\alpha\beta} - R_s i_{\alpha\beta}) \\ J = \begin{bmatrix} 0 & -1 \\ 1 & 0 \end{bmatrix} \\ H = \begin{bmatrix} 1 & \dfrac{\rho}{\omega_r} \\ -\dfrac{\rho}{\omega_r} & 1 \end{bmatrix} \end{cases} \tag{15}$$

The structure of the state observer is shown in Fig. 5.

In the above state observer, the PMSM parameters R_s and L_q are used, and they are defined as $\hat{R}_s$ and $\hat{L}_q$. Therefore, the parameter dependence problem should be discussed. Accroding to the first equation of Equ. (14), the following equation is established in the flux observation process:

$$u_{\alpha\beta} = \hat{R}_s i_{\alpha\beta} + \hat{L}_q D i_{\alpha\beta} + D\hat{\psi}_{e\alpha\beta} \tag{16}$$

Then, the following equation can be obtained:

$$\int (u_{\alpha\beta} - \hat{R}_s i_{\alpha\beta})dt = \hat{L}_q i_{\alpha\beta} + \hat{\psi}_{e\alpha\beta} \tag{17}$$

Obviously, the left part of Equ. (17) is the flux formula based on the stator voltage model. The right part of Equ. (17) is the estimated stator flux in this paper.

$$\begin{cases} \psi_{\alpha\beta} = \hat{L}_q i_{\alpha\beta} + \hat{\psi}_{e\alpha\beta} \\ \boldsymbol{\psi}_s = \psi_\alpha + j\psi_\beta \end{cases} \tag{18}$$

Equ. (16) is always established, hence the observation

accuracy of Equ. (18) is independent of the PMSM inductance parameters. It only depends on the stator resistance. Moreover, central 60° synchronous modulation is employed when the motor speed is relatively high. The influence of the stator resistance R_s can be ignored under such conditions. Thus, the stator flux $\boldsymbol{\psi}_s$ observed by Equ. (18) is practical and almost independent of the PMSM parameters.

C. Dynamic Flux Error Elimination and Modulation Correction

As previously defined, the dynamic flux error $d\psi(t)$ is the difference value between the target and actual stator flux. Therefore:

$$d\psi(t) = \psi_{ss}(t) - \psi_s(t) \tag{19}$$

The dynamic flux error $d\psi(t)$ is used in a trajectory controller to modify the actual pulse pattern $P(\beta, N)$ so that $d\psi(t)$ is minimized, and ultimately reduced to zero. The required elimination component $\Delta\psi_{ss}(t)$ of the target stator flux is the inverse of the existing error, which means:

$$\Delta\psi_{ss}(t) = -d\psi(\mathrm{t}) \tag{20}$$

According to the stator flux calculation, $d\psi(t)$ is a volt-second error. Therefore, the error can be eliminated by adjusting the switching instants, ahead or lagging in time, of the original pulse sequence within the current sampling interval under consideration. For ease of explanation and formula expression, the relevant variables and physical processes of a two-level inverter are defined as follows:

(1) The converter bridge arm switch state is marked by S. S_A, S_B, and S_C, correspond to the A, B, and C three-phase, respectively. When the upper bridge arm is on, $S = 1$. When the lower bridge arm is on, $S = 0$.

(2) The voltage level change is marked by s. s_a, s_b, and s_c, correspond to the three-phases, respectively. When the voltage level changes from $-U_{dc}/2$ to $U_{dc}/2$, $s = 1$. When the voltage level changes from $U_{dc}/2$ to $-U_{dc}/2$, $s = -1$. There may be more than one switching instant in a sampling interval for a given phase. Then the subscript 'i' in 's_i' is used to distinguish them as serial number. The absence of voltage steps in a sampling interval for a given phase is marked by $s = 0$.

(3) Adjusting the time of a switching instant is marked by Δt. $\Delta t > 0$ when a switching instant is advanced. $\Delta t < 0$ when a switching instant is delayed. If the volt-second contribution of a certain phase needs to be increased, the switching instant should be advanced with $\Delta t > 0$ when $s_i = 1$, and the switching instant should be delayed with $\Delta t < 0$ when $s_i = -1$. If the volt-second contribution of a certain phase needs to be decreased, the switching instant should be delayed with $\Delta t < 0$ when $s_i = 1$, and the switching instant should be advanced with $\Delta t > 0$ when $s_i = -1$.

A sketch map of the definitions of the variables and physical processes is shown in Fig. 6.

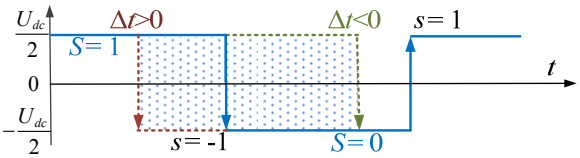

Fig. 6. Definition of relevant variables and physical processes in modulation correction.

According to the principle of two-level inverters, the phase voltages can be deduced from the bridge arm switch states:

$$\begin{cases} u_{an} = \frac{1}{3}\cdot U_{dc}\cdot(2S_A - S_B - S_C) \\ u_{bn} = \frac{1}{3}\cdot U_{dc}\cdot(2S_B - S_A - S_C) \\ u_{cn} = \frac{1}{3}\cdot U_{dc}\cdot(2S_C - S_A - S_B) \end{cases} \tag{21}$$

The dynamic modulation flux error $d\psi(t)$ presents as three components $d\psi_a(t)$, $d\psi_b(t)$ and $d\psi_b(t)$ in the three-phase stationary coordinate system as:

$$\begin{cases} d\psi_a(t) = d\psi(t)\cdot\mathbf{1} \\ d\psi_b(t) = d\psi(t)\cdot\boldsymbol{a} \\ d\psi_c(t) = d\psi(t)\cdot\boldsymbol{a}^2 \end{cases} \tag{22}$$

where, $\mathbf{1}$, $\boldsymbol{a}$ and $\boldsymbol{a}^2$ are the unity vectors in the direction of the A-phase, B-phase and C-phase axis respectively. According to Equ. (21), the phase time adjustments Δt_{ai}, Δt_{bi} and Δt_{ci} of the existing i transitions within the sampling interval change the corresponding phase flux error respectively by:

$$\begin{cases} \Delta d\psi_a(t) = \frac{2}{3}\cdot U_{dc}\cdot\sum_{i=0}^{n} s_{ai}\Delta t_{ai} \\ \Delta d\psi_b(t) = \frac{2}{3}\cdot U_{dc}\cdot\sum_{i=0}^{n} s_{bi}\Delta t_{bi} \\ \Delta d\psi_c(t) = \frac{2}{3}\cdot U_{dc}\cdot\sum_{i=0}^{n} s_{ci}\Delta t_{ci} \end{cases} \tag{23}$$

When using Δt_{ai}, Δt_{bi} and Δt_{ci} to eliminate the dynamic flux error $d\psi(t)$; according to Equ. (20), (22) and (23); Δt_{ai}, Δt_{bi} and Δt_{ci} can be obtained by:

$$\begin{cases} \Delta t_{ai} = -\frac{3}{2U_{dc}}\cdot\frac{1}{s_{ai}}\cdot d\psi_a(t) \\ \Delta t_{bi} = -\frac{3}{2U_{dc}}\cdot\frac{1}{s_{bi}}\cdot d\psi_b(t) \\ \Delta t_{ci} = -\frac{3}{2U_{dc}}\cdot\frac{1}{s_{ci}}\cdot d\psi_c(t) \end{cases} \tag{24}$$

Equs. (21)-(24) are the theoretical foundation of dynamic flux error elimination in the three-phase stationary coordinate system. The principle of this method is that the flux error of a particular phase is mainly eliminated by the phase time adjustments. This method has two disadvantages:

(1) The time adjustments of a particular phase do not exert an effect exclusively on that phase component of the dynamic flux error. This is easy to understand according to Equ. (21). The mutual coupling between the three-phase time adjustments causes difficulties for accurate flux error

elimination.

(2) If no voltage level change exists in the modulation pattern of a given phase in a sampling interval, that particular phase component of the dynamic flux error is less effectively changed by interfering with the patterns of the other two phases. However, the above method cannot offer clear theoretical guidance for such a situation.

Some improvements are carried out based on the above flux error elimination principle. Dynamic flux error elimination will be discussed in the α-β stationary coordinate system. In this coordinate system, the two-phase voltage can be deduced from the bridge arm switch states of a two-level inverter:

$$\begin{cases} U_\alpha = \frac{1}{3}\cdot U_{dc}\cdot(2\cdot S_A - S_B - S_C) \\ U_\beta = \frac{\sqrt{3}}{3}\cdot U_{dc}\cdot(S_B - S_C) \end{cases} \tag{25}$$

According to Equ. (18) and (25), the three-phase time adjustments Δt_{ai}, Δt_{bi} and Δt_{ci} of the existing i transitions within the sampling interval change the total dynamic flux error by $\Delta d\psi(t)$:

$$\begin{aligned} \Delta d\boldsymbol{\psi}(t) &= \Delta d\psi_\alpha(t) + j\Delta d\psi_\beta(t) \\ &= \frac{1}{3}\cdot U_{dc}\cdot\sum_{i=1}^{n}\begin{bmatrix}(2s_{ai}\Delta t_{ai} - s_{bi}\Delta t_{bi} - s_{ci}\Delta t_{ci}) \\ +j\sqrt{3}(s_{bi}\Delta t_{bi} - s_{ci}\Delta t_{ci})\end{bmatrix} \end{aligned} \tag{26}$$

In the α-β stationary coordinate system, $d\psi(t)$ is decomposed into two components $d\psi_\alpha(t)$ and $d\psi_\beta(t)$. The following inferences can be obtained by Equ. (26):

(1) Δt_{ai} only affects $d\psi_\alpha(t)$, it does not affect $d\psi_\beta(t)$.

(2) Δt_{bi} effects $d\psi_\alpha(t)$ and $d\psi_\beta(t)$ with different trends.

(3) Δt_{ci} has the same influence trend on $d\psi_\alpha(t)$ and $d\psi_\beta(t)$.

Therefore, based on Equ. (26) and the above inferences, the follow dynamic flux error elimination rules are set up in the α-β coordinate system. For a simple description of the formulas, assume that $d\psi(t)$ is eliminated by the switching instant i.

(1) If the dynamic flux error has only an α-phase component, the A-phase switching pattern is modified to eliminate $d\psi_\alpha(t)$.

$$\begin{cases} \Delta t_{ai} = -\frac{3}{2U_{dc}}\cdot\frac{1}{s_{ai}}\cdot d\psi_\alpha(t) \\ \Delta t_{bi} = 0 \\ \Delta t_{ci} = 0 \end{cases} \tag{27}$$

(2) If $d\psi_\alpha(t)$ and $d\psi_\beta(t)$ are positive or negative respectively, the B-phase switching pattern is modified to eliminate them simultaneously.

$$\begin{cases} \Delta t_{ai} = \frac{-3}{2U_{dc}}\cdot\frac{1}{s_{ai}}\cdot(d\psi_\alpha(t) + \frac{d\psi_\beta(t)}{\sqrt{3}}) \\ \Delta t_{bi} = \frac{-\sqrt{3}}{U_{dc}}\cdot\frac{1}{s_{bi}}\cdot d\psi_\beta(t) \qquad ,|d\psi_\alpha(t)| > \frac{|d\psi_\beta(t)|}{\sqrt{3}} \\ \Delta t_{ci} = 0 \end{cases} \tag{28}$$

$$\begin{cases} \Delta t_{ai} = 0 \\ \Delta t_{bi} = \frac{3}{U_{dc}}\cdot\frac{1}{s_{bi}}\cdot d\psi_\alpha(t), \qquad |d\psi_\alpha(t)| < \frac{|d\psi_\beta(t)|}{\sqrt{3}} \\ \Delta t_{ci} = 0 \end{cases} \tag{29}$$

(3) If $d\psi_\alpha(t)$ and $d\psi_\beta(t)$ are positive or negative similarly, the C-phase switching pattern is modified to eliminate them simultaneously.

$$\begin{cases} \Delta t_{ai} = \frac{-3}{2U_{dc}}\cdot\frac{1}{s_{ai}}\cdot(d\psi_\alpha(t) - \frac{d\psi_\beta(t)}{\sqrt{3}}) \\ \Delta t_{bi} = 0 \qquad ,|d\psi_\alpha(t)| > \frac{|d\psi_\beta(t)|}{\sqrt{3}} \\ \Delta t_{ci} = \frac{\sqrt{3}}{U_{dc}}\cdot\frac{1}{s_{ci}}\cdot d\psi_\beta(t) \end{cases} \tag{30}$$

$$\begin{cases} \Delta t_{ai} = 0 \\ \Delta t_{bi} = 0 \qquad , \qquad |d\psi_\alpha(t)| < \frac{|d\psi_\beta(t)|}{\sqrt{3}} \\ \Delta t_{ci} = \frac{3}{U_{dc}}\cdot\frac{1}{s_{ci}}\cdot d\psi_\alpha(t) \end{cases} \tag{31}$$

New errors are undesirable in the elimination of the original error. Δt_{ai}, Δt_{bi} and Δt_{ci} are limited by the length of the sampling interval. It is possible that there is no voltage level change of a given phase in the current sampling interval. Therefore, a particular $d\psi(t)$ often cannot be completely eliminated in a sampling interval. Modifying the three-phase switching patterns by Δt_{ai}, Δt_{bi} and Δt_{ci} decided by Equs. (27)-(31), the dynamic flux $d\psi(t)$ will be completely eliminated after a number of sampling intervals.

IV. Simulation and Experiment

Compared to the original central 60° synchronous modulation, the modified one with the PMSM stator flux trajectory control is proposed to improve the transient responses and to guarantee smooth modulation mode switching. The feasibility and advantages of the proposed method are verified on a PMSM experimental platform in this paper. The experimental platform includes a voltage regulator, a converter, a 5.5kW PMSM, a TMS320F28335 digital controller, a load system and other parts. The platform components are shown in Fig. 7.

The main parameters of the experimental PMSM are shown in Table I. Due to limitations of the laboratory conditions, the experimental platform power level is relatively smaller than that of actual train drive systems. However, this factor does not affect the validity of the proposed method. In this paper, the switching frequency is controlled at a level less than 500Hz in the SVPWM and less than 230Hz in the central 60° synchronous modulation. The actual modulation modes can be simulated under similar conditions.

A. Simulation

Simulation models are built in Matlab/Simulink employing the parameters shown in Table I. Utilizing the original

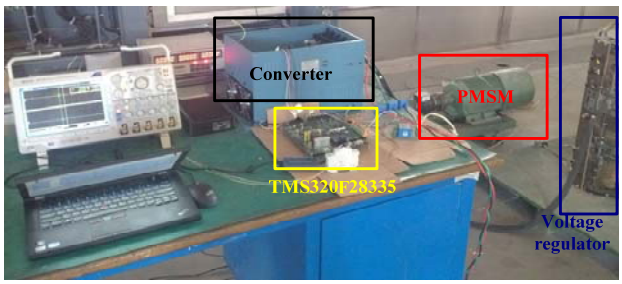

Fig. 7. Experimental platform components.

TABLE I
PARAMETERS OF EXPERIMENTAL PMSM

Rated power	5.5/kW
Rated voltage	380/V
Rated current	13/A
Rated speed	1500r/min
Rated torque	35 Nm
Pole pairs	2
Winding resistance	1.3Ω
q-axis inductance	100mH
d-axis inductance	50mH
Rotor flux	1.25Wb

central 60° synchronous modulation and the proposed one with the PMSM stator flux control, the following simulation operation is designed. The entire simulation time is 5 seconds. The PMSM accelerates uniformly from 0 to 32HZ in 3.2s. Then it runs at a constant velocity. The modulation mode changes from the SVPWM to the central 60° synchronous modulation when the motor stator frequency is 27.5Hz at about 2.75s. The load torque steps from 35Nm to 25Nm at 4s. In order to output the rated torque of 35Nm on the basis of a simple motor control, the d-axis current is controlled at -5A during the whole process. The speeds, torques, q-axis currents and d-axis currents are shown in Fig. 8 from top to bottom. Fig. 8(a), the left side of Fig. 8, shows the results of the proposed method. Fig. 8(b), the right side of Fig. 8, shows the results of the original method.

When the modulation mode changes to the central 60° synchronous modulation at 2.75s, the torque impact noticeably rises with the original central 60° synchronous modulation and does not appear after adding the stator flux control. There are three steps of the output torque. The motor starts with a load torque of 35Nm, acceleration ends at 3.2s, and the load torque steps at 4s. The torque response is significantly better under the stator flux control. Its output torque keeps up with the command value quickly and without oscillations at 4s. Like the torque responses, the current responses with the PMSM stator flux control present a smaller impact on the modulation mode switch at 2.75s, a lighter oscillation when the acceleration ends at 3.2s and load torque steps at 4s.

Although the control system processes the trajectory of the

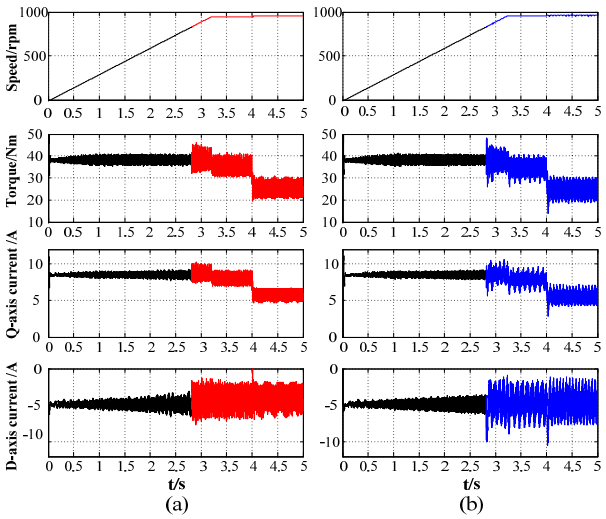

Fig. 8. Simulated speeds, torques, q-axis and d-axis currents. (a) Results of the proposed method, (b) results of the original one.

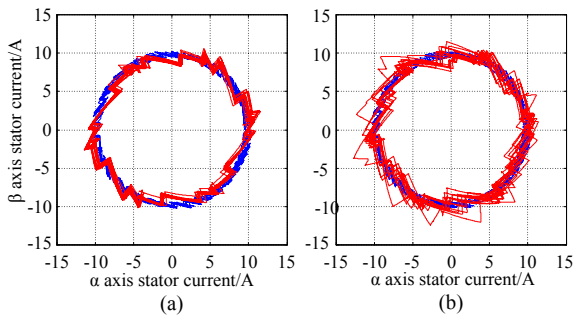

Fig. 9. Simulated stator current vector trajectories around modes switch point. (a) Result of the proposed method, (b) result of the original method.

stator flux vector, the trajectories of the stator current vector show the distortions to be more pronounced. They were recorded for better insight. Fig. 9 shows the stator current vector trajectories around mode switching point. The blue curves are the current trajectories with the SVPWM; the red curves are the current trajectories after the modulation mode change and in subsequent acceleration. Obviously, the current trajectory with the stator flux trajectory control changes softer when the modulation mode changes. The current trajectory of the original central 60° synchronous modulation impacts and fluctuates severely. The stator current vector trajectories around the load torque step at 4.0s are shown in Fig. 10. The blue curves are the current trajectories bearing the load torque 35Nm; the red curves are the trajectories after the load torque step and bearing 25Nm. With the stator flux trajectory control, the current trajectory changes placidly and definitely without an impact. Current trajectories of a different load capacity did not intertwine.

The simulation results show that the modified central 60° synchronous modulation with the PMSM stator flux control is feasible, and that the performance improvement is remarkable.

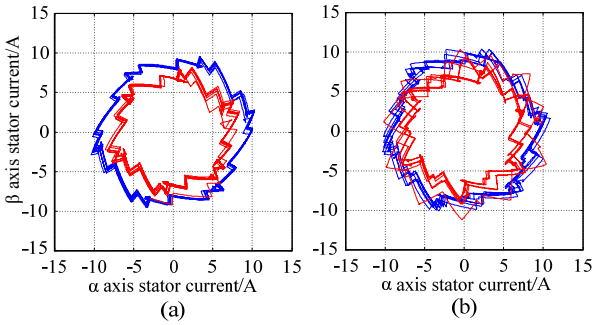

Fig. 10. Simulated stator current vector trajectories around load torque step. (a) Result of the proposed method, (b) result of the original method.

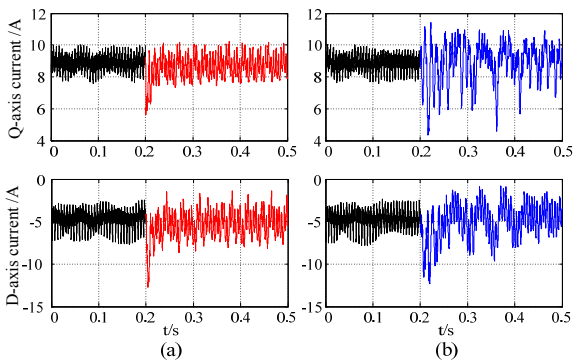

Fig. 11. Experimental q-axis and d-axis currents around modes switch point. (a) Results of the proposed method, (b) results of the original one.

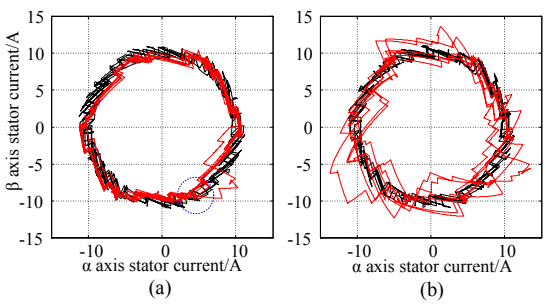

Fig. 12. Experimental stator current vector trajectories around modes switch point. (a) Results of the proposed method, (b) results of the original one.

B. Experiment

The specific experiment process is as follows: The load torque increased to the rated torque 35 Nm gradually when the PMSM runs at 10 HZ. Then the PMSM stator frequency accelerates evenly from 10Hz to 32Hz in 2.2s. The modulation mode changes from the SVPWM to the central 60° synchronous modulation when stator frequency is 27.5Hz. Finally, the load torque steps from 35Nm to 25Nm when the PMSM runs at 32 HZ. The d-axis current is controlled at -5A during the whole process. The Central 60° synchronous modulation with the PMSM stator flux control and the original control are both used.

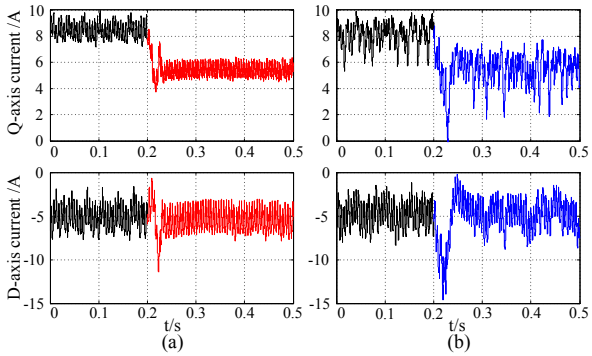

Fig. 13. Experimental q-axis and d-axis currents around load torque step. (a) Results of the proposed method, (b) results of the original one.

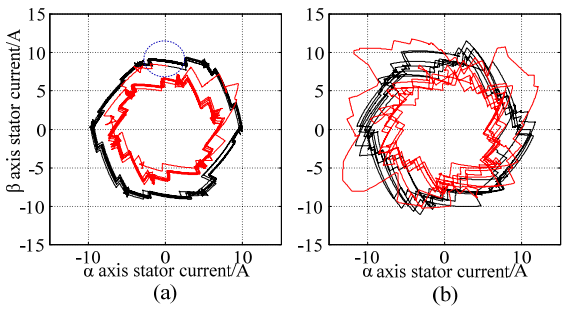

Fig. 14. Experimental stator current vector trajectories around load torque step. (a) Results of the proposed method, (b) results of the original one.

The experimental q-axis and d-axis currents, and the stator current vector trajectories around the mode switching point are shown in Fig. 11 and 12, respectively.

In Fig. 11, the black curves are the currents before modulation mode change, and the colorized curves are the currents after the modulation mode change. Although there is a current impact in Fig. 11(a) with the stator flux trajectory control, the impact is eliminated quickly. However, the currents of the original method fluctuate continuously, and cannot be stabilize quickly.

In Fig. 12, the black curves are the current trajectories before the modulation mode change and the red curves are the current trajectories after modulation mode change. In Fig. 12(a), with the stator flux control, the trajectory excursion is small and eliminated quickly. It is eliminated in about a quarter of a cycle. In Fig. 12(b), without the stator flux control, the trajectory excursion is large and lasts for a long time. Apparently, it is a smoother modulation mode switching with the stator flux trajectory control.

Experimental q-axis and d-axis currents around the load torque step are shown in Fig. 13, and stator current vector trajectories are shown in Fig. 14.

In Fig. 13, the black curves are the currents before load torque step, and the colorized curves are the currents after load torque step. A smaller d-axis and q-axis current shock is guaranteed and it can be eliminated quickly by the stator flux

trajectory control. In Fig. 14, the black curves are the current trajectories before the load torque step, and the red curves are the current trajectories after the load torque step. In Fig. 14(a), with the stator flux control, the current trajectory has a smooth transition. In addition, the trajectory excursion is eliminated in about one cycle. In Fig. 14(b), without the stator flux control, the trajectory fluctuates violently. The large excursion of the stator current vector would have caused an over-current trip if the system had less of a current margin.

The feasibility and advantages of the proposed method are also verified by platform experiments.

V. CONCLUSION

Traditional central 60° synchronous modulation is easily achieved for train traction inverters as a special PWM when the equivalent carrier ratio is relatively low. The switching patterns of the traditional central 60° modulation are calculated for every steady-state operating point. Consequently, the continuity of the target and actual harmonic currents is challenged and a poor transient response is encountered when the operating conditions change. The stator flux control is added to solve this problem. Moreover, the stator flux control is extended to ensure smooth mode switching between the central 60° synchronous modulation and the SVPWM.

Based on an electrical model of a two-level three-phase inverter and PMSM, the calculation of the target stator flux, the observation of the actual PMSM stator flux, and the modification rules of the original switching pattern are deduced and described. A minimum order flux state observer based on the extended flux model is referenced, and determined to be almost independent of the PMSM parameters in the background of this paper. In order to achieve a faster and more accurate flux trajectory tracking, the dynamic flux error elimination is discussed in the α-β coordinate system. Compared to the discussion in the three-phase coordinate system, more specific compensation rules are obtained. The new compensation rules are universal, and can be extended to techniques such as the SHE-PWM with stator flux control.

With a switching frequency of less than 230Hz, the feasibility and advantages of the proposed method are verified by simulation and experimental results.

REFERENCES

[1] J. Holtz and X. Qi, "Optimal control of medium-voltage drives-An overview," *IEEE Trans. Ind. Electron.*, Vol. 60, No. 12, pp. 5472-5481, Dec. 2013.

[2] R. Rathore, H. Holtz, and T. Boller, "Generalized optimal pulsewidth modulation of multilevel inverters for low-switching-frequency control of medium-voltage high-power industrial AC drives," *IEEE Trans. Ind. Electron.*, Vol. 60, No. 10., pp. 4215-4224, Oct. 2013.

[3] J. Napoles, J. I. Leon, R. Portillo, L. G. Franquelo, and M. A. Aguirre, "Selective harmonic mitigation technique for high-power converters," *IEEE Trans. Ind. Electron.*, Vol. 57, No. 7, pp. 2315-2323, Jul. 2010.

[4] S. R. Bowes and D. Holliday, "Optimal regular-sampled PWM inverter control techniques," *IEEE Trans. Ind. Electron.*, Vol. 54, No. 3, pp. 1547-1559. Jun. 2007.

[5] M. Zhou, X. You, and C. Wang, "Research on PWM method under low switching frequency," *Journal of Beijing Jiaotong University*, Vol. 34, No. 5, pp. 53-57, Oct. 2010.

[6] W. Li, X. Che, and R. Hao, "Research on PWM method for AC-DC-AC electric locomotive," *Journal of the China Railway Society*, Vol. 22, No. 6, pp. 26-31, Dec. 2000.

[7] J. Holtz and B. Beyer, "Optimal synchronous pulsewidth modulation with a trajectory-tracking scheme for high-dynamic performance," *IEEE Trans. Ind. Appl.*, Vol. 29, No. 6, pp. 1098-1105, Nov./Dec. 1993.

[8] J. Holtz and B. Beyer, "Fast current trajectory control based on synchronous optimal pulsewidth modulation," *IEEE Trans. Ind. Appl.*, Vol. 31, No. 5, pp. 1110-1120, Sep./Oct. 1995.

[9] J. Holtz and N. Oikonomou, "Fast dynamic control of medium voltage drives operating at very low switching frequency: an overview," *IEEE Trans. Ind. Electron.*, Vol. 55, No. 3, pp. 1005-1013, Mar. 2008.

[10] J. Holtz and N. Oikonomou, "Synchronous optimal pulsewidth modulation and stator flux trajectory control for medium-voltage drives," *IEEE Trans. Ind. Appl.,* Vol. 43, No. 2, pp. 600-608, Mar./Apr. 2007.

[11] Y. Wang, X. Wen, X. Guo, F. Zhao, and W. Cong, "The smooth transition research of different PWM modulations for vector control of induction motor in medium voltage high power," in *International Conference on Electrical Machines and Systems(ICEMS)*, pp. 1-5, Aug. 2011.

[12] X. Ma, J. Ren, Q. Ge, and Y. Li, "Full speed range induction motor indirect rotor field oriented control for high speed traction applications," in *International Conference on Electrical Machines and Systems(ICEMS)*, pp. 1407-1412, Oct. 2010.

[13] W. Wang, M. Cheng, B. Zhang, Y. Zhu, and S. Ding, "A fault-tolerant permanent magnet traction module for subway application," *IEEE Trans. Power Electron.*, Vol. 29, No. 4, pp. 1646-1658, Apr. 2014.

[14] M. Mekhiche, S. Nichols, J. L. Kirtley, and J. Young, "High-speed, high-power density PMSM drive for fuel cell powered HEV application," in *IEEE International Electrical Machines and Drives Conference(IEMDC)*, pp. 658-663, Jun. 2001.

[15] S. Shinnaka, "New sensorless vector control methods based on a new minimum-order flux state-observer in the "D-Module" for permanent magnet synchronous motors," *Electrical Engineering in Japan*, Vol. 151, No. 2, pp. 46-62, Apr. 2005.

Xiaochun Fang was born in Jiangxi Province, China, in 1987. He received his B.S. degree in Electrical Engineering and Automation from Beijing Jiaotong University, Beijing, China, in 2010. He is presently working towards his Ph.D. degree in Electrical Engineering and Automation at Beijing Jiaotong University, Beijing, China. His current research interests include electric traction systems for rail vehicles.

Fei Lin was born in Shandong Province, China, in 1975. He received his B.S. degree in Electrical Engineering from Xi'an Jiaotong University, Xi'an, China, in 1997; his M.S. degree in Electrical Engineering from Shandong University, Shandong, China, in 2000; and his Ph.D. degree in Electrical Engineering from Tsinghua University, Beijing, China, in 2004. Since 2004, he has been with School of Electrical Engineering, Beijing Jiaotong University, Beijing, China, where he is presently working as an Associate Professor. His current research interests include power electronics and motor control.

Zhongping Yang was born in Chongqing, China, in 1971. He received his B.S. degree in Electrical Engineering from the Tokyo University of Mercantile Marine, Tokyo, Japan, in 1997; and his M.S. and Ph.D. degrees in Electrical Engineering from the University of Tokyo, Tokyo, Japan, in 1999 and 2002, respectively. He is presently working as a Professor in the School of Electrical Engineering, Beijing Jiaotong University, Beijing, China. His current research interests include high-speed rail systems, traction and regenerative braking technologies, and wireless power transfer for light rail vehicles.